Observation of spiral pattern and spiral defect chaos in dielectric barrier discharge in argon/air at atmospheric pressure

Lifang Dong,* Fucheng Liu, Shuhua Liu, Yafeng He, and Weili Fan
College of Physics Science & Technology, Hebei University, Baoding, 071002, China
(Received 1 November 2004; published 21 October 2005)

A rich variety of spiral patterns such as single-armed spiral, dipole spirals, target pattern, multiarmed spiral, and spiral defect chaos state have been observed in ac-driven atmospheric pressure gas discharge. The confined and free boundary conditions are defined by means of whether there is a sidewall in the discharge domain or not, respectively. In the free boundary condition, the spiral pattern arises when the stripe pattern undergoes core instability or notching instability. In the confined boundary condition, the spiral pattern is formed by sidewall forcing. The spiral drifts upward in the free boundary condition and meanders in the confined boundary condition. The topological charge of the spiral pattern can be changed when the spiral interacts with the dislocations. The spiral wavelength (average distance between two consecutive rolls) is a function of gas composition and decreases rapidly with increase of air concentration in discharge gas.

DOI: 10.1103/PhysRevE.72.046215 PACS number(s): 82.40.Bj, 47.54.+r, 52.80.Tn

I. INTRODUCTION

Spiral patterns are fascinating patterns that have been observed in many systems of different origins such as chemical [1], biological [2], and physical systems [3–6]. In recent years, it has been found that the spirals in cardiac muscle play an essential role in heart diseases such as arrhythmia and fibrillation, the latter being the leading cause of death in the industrialized world.

The physical systems generally used for studying spiral pattern are the Rayleigh-Benard convection (RBC) [3,4] and "Faraday experiment" of fluid or sand [5,6]. The Rayleigh-Benard convection is a well-established model system in which the pattern is driven by the temperature difference across the fluid layer. Theoretically, the spiral state is successfully reproduced by numerical simulation of the generalized Swift-Hohenberg model coupled to a self-consistent large-scale flow [7]. The spiral pattern forms when the stripe pattern undergoes some instability. Core instability is an accustomed instability, which has been observed in experiments [3] and in simulations [8]. Notching instability is proposed in the simulations and still needs the experimental evidence [9]. Another nonlinear system for studying the spiral pattern is the "Faraday experiment", in which the fluid or sand is driven by sinusoidal vertical oscillations. In this system, the sidewall forcing plays an essential role in the spiral formation.

As a new type of pattern formation system, dielectric barrier discharge (DBD) has been paid much attention [10–15]. DBD (also referred to as silent discharge) is a typical nonequilibrium gas discharge. It has been widely used in industrial fields such as ozone generation and large-area flat plasma display panels (PDP) [16]. An experimental device for DBD generally consists of two parallel electrodes—at least one covered with a thin dielectric layer. An ac voltage is applied to the electrodes at a frequency of several hundreds Hz to a few 100 kHz. Breakdown occurs in the gas gap between electrodes at a sufficiently high voltage, and a transient discharge initiates during each half cycle of the voltage. The discharges appear in different types depending on the experimental conditions, especially on the product pd of pressure p and gas gap width d. For a low product pd (usually less than 10 Torr cm), the discharge operates in Townsend breakdown and appears in uniform transient glow discharge [11]. For a high product pd, the discharge operates in a streamer regime leading to the formation of narrow discharge filaments. DBD generally is an essentially nonlinear process due to the nonlinear charge conduction process in gas and the accumulated charges on dielectric surface [10]. Various pattern formations such as stripe pattern, hexagon pattern, concentric ring pattern, and square pattern have been observed in DBD [10–15]. Also a target pattern was observed in the DBD system under the condition that pd value is less than 4 Torr cm. Recently single-armed spiral patterns have been observed in dc-driven gas discharge in low pd value [17,18]. However, to the best of our knowledge, there is no report on the observation of multiple-armed spiral and spiral defect chaos in DBD.

In addition, DBD has the unique advantage that it has a light emission feature, which leads to an important fact that the spatiotemporal dynamics of patterns can be studied experimentally. For example, it is found that the square pattern in DBD is an interleaving of two square patterns, and the sequence of two patterns' appearance is changed alternately by measuring the spatiotemporal correlations between discharge filaments [13]. Another example, the concentric ring pattern, is a superposition of two ring patterns by measuring pattern dynamics [12]. These results are of great importance to the study of pattern dynamics. Therefore, the knowledge of spiral dynamics will be greatly enriched if a spiral pattern can be realized in DBD.

In this work, we report an observation of various types of spiral patterns and spiral defect chaos (SDC) state in DBD. The dynamics of spiral patterns in two different time scales is studied. The forming process and evolution of spiral pat-

*Electronic address: Donglf@mail.hbu.edu.cn

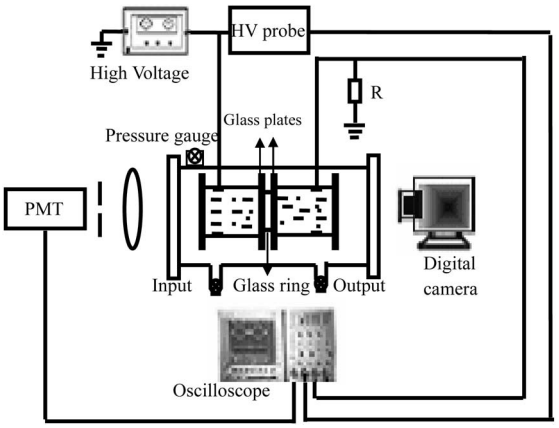

FIG. 1. Schematic diagram of the experimental setup with sidewall.

terns under two different boundary conditions are investigated. The results show that the DBD system is an excellent system for studying spiral patterns.

In the following, Sec. II contains the description of the experimental setup including the water electrodes we adopted and the definition of boundary conditions. Our experimental results, including various types of spiral patterns, spiral formation, interactions between spirals and dislocations, and variation of spiral wavelength, are presented in Sec. III. A brief conclusion will be given in Sec. IV.

II. EXPERIMENTAL SYSTEM

The experimental device is shown in Fig. 1. Two cylindrical containers, with diameters of 65 mm, sealed with 1.5 mm thick glass plates, are filled with water. There is a metallic ring immersed in each of the containers and connected to a power supply. Thus the water acts as a liquid electrode. The glass plates serve as a dielectric layer. All of the apparatus is enclosed in a big container filled with a mixture of argon and air. The gas pressure is kept at atmospheric pressure. The temperature of the input gas is at room temperature (291–293 K), while the initial electrodes are cooled down to about 281 K or lower. A sinusoidal ac voltage at frequency of 60 kHz is applied to the electrodes. A high-voltage probe (Tektronix P6015A 1000X) is used to measure the applied voltage. The light emission of the discharge filaments is detected by a PMT (RCA7265) and recorded with an oscilloscope (Tektronix TDS3054B, 500MHz). A digital camera (Canon Powershot G1) is used to take the picture of the patterns.

The gas gap of the inner parallel glass plates can be adjusted from 0.1 to 2.0 mm. Two kinds of gas boundary conditions, hereafter designated as the free boundary condition and the confined boundary condition, respectively, are designed in our experiments. In the free boundary condition, the gap is laterally free and the discharge gas can exchange with the ambient gas freely. In contrast, a circular (or rectangular) glass ring with the diameter (or diagonal) of 60 mm served as sidewall limits the diffusion of the discharge gas laterally in the confined boundary condition.

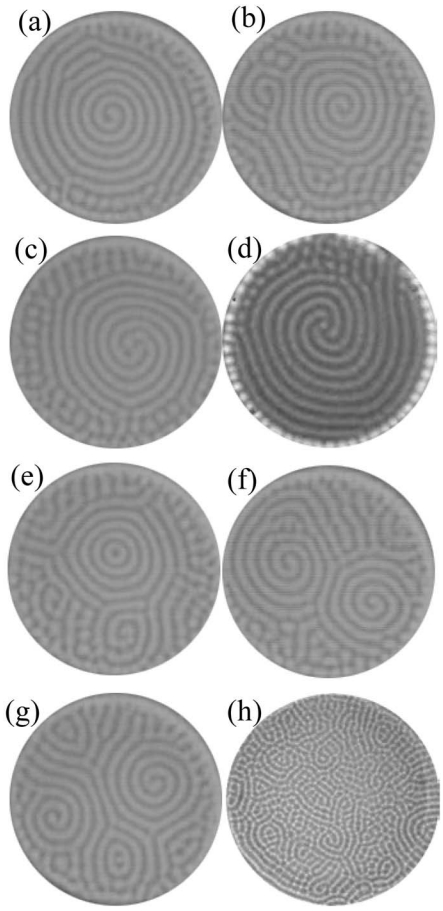

FIG. 2. Various spiral patterns: (a) single-armed spiral with counterclockwise winding (U=3100 V, χ=1.16%); (b) single-armed spiral with clockwise winding (U=3100 V, χ=1.16%); (c) double-armed spiral (U=3100 V, χ=1.16%); (d) triple-armed spiral (U=5200 V, χ=0.91%); (e) target (U=3100 V, χ=1.16%); (f) dipole with same winding (U=3100 V, χ=1.16%); (g) dipole with opposite winding (U=3100 V, χ=1.16%); (h) spiral defect chaos (U=8500 V, χ=4.96%). The other parameters: p=760 Torr, d=1.4 mm, f=60 kHz, and t_{exp}=40 ms. The free boundary condition has been used in (a), (b), (c), (e), (f), and (g) (the diameter of discharge area is 65 mm) and the confined boundary condition has been used in (d) and (h) (the diameter of discharge area is 60 mm).

III. EXPERIMENTAL RESULTS

A. Various spiral patterns

A variety of spiral patterns have been observed in our experiments over the following range of parameters: the pd value is in the range of 80–150 Torr cm (i.e., the discharge is in streamer regime), the air concentration χ in discharge gas is changed from 0.91% to 4.96%. The spiral patterns observed include individual spirals with different chirality (the rotation direction of the spiral) [Figs. 2(a) and 2(b)], double-armed spiral [Fig. 2(c)], triple-armed spiral [Fig. 2(d)], targets [Fig. 2(e)], dipoles with the same or opposite windings [Figs. 2(f) and 2(g)], and spiral defect chaos [Fig. 2(h)].

Figure 3 gives the temporal behavior of the spiral pattern in different time scales. The consecutive images of the spiral pattern have been taken every 1/15 second, which gives the

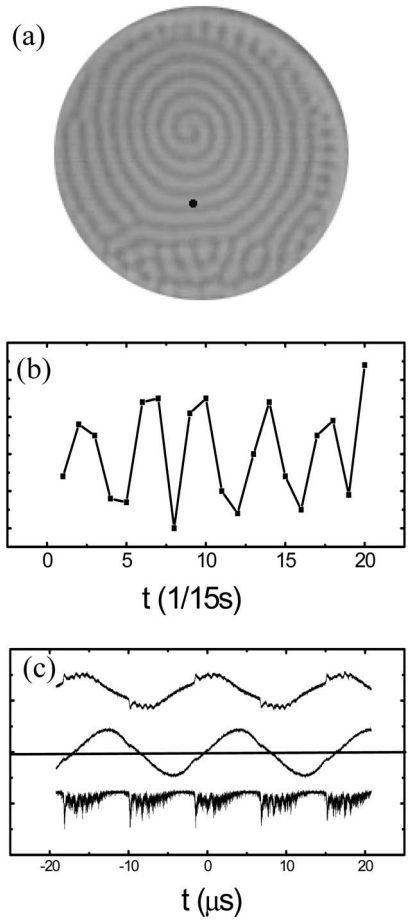

FIG. 3. Temporal behavior of the spiral pattern in different time scales. (a) A single-armed spiral pattern (U=3100 V, χ=1.16%, p=760 Torr, d=1.4 mm, f=60 kHz, t_{exp}=40 ms, free boundary condition, and the diameter of discharge area is 65 mm); (b) time evolution of intensity of a fixed point as shown in (a); (c) the waveforms of discharge current (top), voltage (middle), and light emission (bottom) of the spiral in (a).

dynamic behavior of the spiral pattern in one-tenth second scale. The intensity in a fixed point marked in Fig. 3(a) exhibits a periodic temporal evolution as shown in Fig. 3(b), in which the period of the spiral is approximately 1/3 s. The dynamic behavior of the spiral pattern in microsecond scale is obtained by measuring the discharge current and the light emission as shown in Fig. 3(c). An obvious characteristic in Fig. 3(c) is discharge current spikes occurring not only at the rising edge but also at the falling edge of applied voltage, what we called discharge before zero voltage [14]. In DBD, charges created in discharge are accumulated on the surface of a dielectric layer, resulting in an electric field that opposes the applied field. Therefore, the net field is abruptly reduced in a localized region and the discharge expires when the net field falls below the maintaining field. However, when the voltage polarity is changed in the next half cycle, breakdown occurs more readily due to the fact that the charge-induced field is of the same polarity as the applied field. The more charges deposited in the last half cycle, the lower the applied voltage needed for breakdown. When the electric field produced by surface charges is larger than breakdown threshold, it will induce the discharge to occur at the falling edge of applied voltage, i.e., discharge before zero voltage. Thus the accumulated charges have two-sided effects on the discharge: inhibit this discharge event and activate the discharge breakdown in the next half cycle of voltage. From the point of view of the reaction-diffusion model, they act as inhibitor in this discharge event and activator in the next half cycle.

The spiral in our experiments is not a rigid spiral. It not only rotates itself but also drifts or meanders. The spiral drifts upward rapidly in the free boundary condition. The spiral will move out of the discharge domain because of the drifting. The whole spiral breaks down into a disordered state when the tip of the spiral reaches the sidewall. It indicates that the tip determines the dynamics of the spiral pattern. In the confined boundary condition the spiral meanders with a relatively low velocity.

B. Spiral formation

In our experiment, it is found that the formation process of the spiral pattern depends on the boundary conditions. In the case with the free boundary condition, a series of patterns can be obtained via increasing the applied voltage. The bifurcation scenario is transient stochastic filaments–traveling hexagon–traveling square (appearing seldom)–unstable quasicrystal–gridding (appearing sometimes)–stripe (roll)–spiral (or target) – spiral defect chaos. Spiral pattern exists over a range of applied voltage, which is dependent upon the gas composition. The onset decreases, while the range becomes wide, with decrease of air concentration in discharge gas. For examples, the onset is 4000 V for the air concentration of 1.8% and 3100 V for 1.16%, and the ranges are 1800 V and 2400 V, respectively. The patterns observed in confined boundary condition undergo another sequence: transient stochastic filaments–static hexagon–static square (appearing seldom)–stable quasicrystal–chaos–spiral (or target) – stripe–spiral defect chaos. In this case, the onset of applied voltage for spiral appearance is higher than that in the free boundary condition, while the range for spiral pattern existence is smaller than that in the free boundary condition. For example, the onset is 4900 V and the range is only 600 V for the air concentration is 1.8%. The spiral defect chaos state appears when the applied voltage is increased to 6300 V.

In the free boundary condition, the spiral pattern arises when the parallel stripes undergo core instability or notching instability. Figure 4 and Fig. 5 give the examples of these two instabilities.

Figures 4(a) and 4(b) illustrate how the core instability initiates the breakup of a short roll. The individual parts reconnect to create a roll closed on itself, and there will be a new core created in the center of the circular rolls [Figs. 4(c)–4(e)]. The core, therefore, acts as a source for the circular wave, gives rise to an additional concentric roll, and eventually creates the target pattern [Fig. 4(f)]. The concentric roll in the center breaks down. One tip becomes the spiral core while the other glides out of the pattern. Then a single-armed spiral forms [Figs. 4(h)–4(j)]. Such a process is similar to that in the RBC system [3].

In the Rayleigh-Benard convection system, Cross and Tu predicted a notching instability that induces a transition from

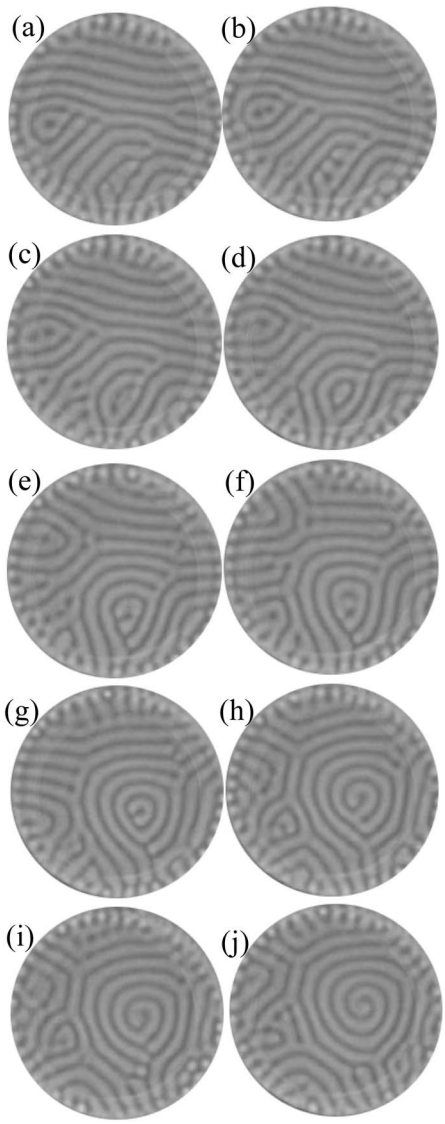

FIG. 4. Transition from stripe to spiral through core instability. Sequence of images: (a) $t=0$ s; (b) $t=1/15$ s; (c) $t=3/15$ s; (d) $t=4/15$ s; (e) $t=6/15$ s; (f) $t=9/15$ s; (g) $t=12/15$ s; (h) $t=1$ s; (i) $t=16/15$ s; (j) $t=17/15$ s. The discharge parameters: $p=760$ Torr, $d=1.7$ mm, $f=60$ kHz, $t_{exp}=40$ ms, $U=3400$ V, $\chi=1.16\%$, and free boundary condition. The diameter of discharge area is 65 mm.

the stripe pattern to a spiral in numerical simulation, which still has not been found in the experiment so far [9,19]. Here we present experimental evidence of this instability. Figure 5 shows an example of this process. The roll in the circled region that has larger wavelength than average wavelength undergoes a short-length scale "notching" instability [Figs. 5(a) and 5(b)], and it has curled up into a spiral [Fig. 5(c)]. The tip of the v-shaped roll becomes the center of the spiral and makes the whole spiral rotate. The spiral becomes larger and larger as it rotates [Fig. 5(d)].

Figure 6 shows how the spiral pattern forms in the confined boundary condition. A ring forms near the sidewall [Figs. 6(a) and 6(b)] when the applied voltage reaches a threshold voltage (about 4200 V in this case), which increases with the increase of air concentration in discharge gas. As the applied voltage increases, additional concentric rolls appear inside until the spiral pattern forms [Fig. 6(c)]. This process is similar to the spiral-forming process in RBC and Faraday system due to sidewall forcing, whose effect is to force the rolls parallel to the boundary sidewall [5,20]. It indicates that sidewall forcing may exist in confined bound-

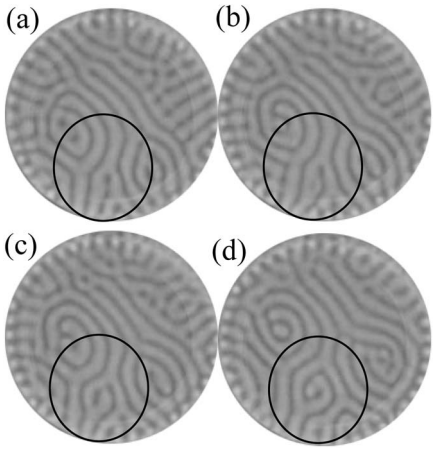

FIG. 5. The forming process of a spiral from a stripe undergoing notching instability. Sequence of images: (a) $t=0$ s; (b) $t=1/15$ s; (c) $t=2/15$ s; (d) $t=5/15$ s. The discharge parameters: $p=760$ Torr, $d=1.7$ mm, $f=60$ kHz, $t_{exp}=40$ ms, $U=3400$ V, $\chi=1.16\%$, and free boundary condition. The diameter of discharge area is 65 mm.

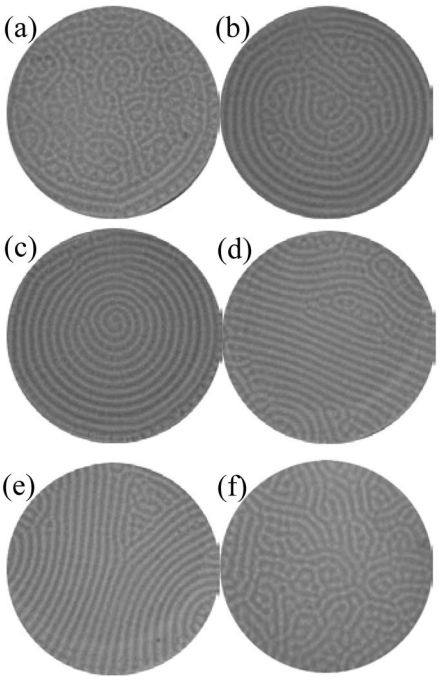

FIG. 6. The forming process of spiral pattern and spiral defect chaos by increasing the applied voltage in confined boundary condition. The voltage: (a) $U=4100$ V; (b) $U=4500$ V; (c) $U=4900$ V; (d) $U=5500$ V; (e) $U=5900$ V; (f) $U=6300$ V. Other parameters: $p=760$ Torr, $d=1.4$ mm, $f=60$ kHz, $t_{exp}=40$ ms, and $\chi=1.8\%$. The diameter of discharge area is 60 mm.

ary conditions although its mechanism is not clear. When the applied voltage increases far away from the threshold voltage, the spiral pattern will lose its stability and change to a parallel stripe pattern [Fig. 6(d)]. Continuing away from the threshold voltage, the number of dislocations and the stripe curvature increase, resulting in grain boundaries and additional sidewall foci. Sufficiently far from onset, spiral defect chaos state [Fig. 6(f)] forms.

C. Change of the topological charge of spiral pattern

The topological charge σ is a parameter describing the chirality of the spiral and the number of the spiral arms. The sign of the topological charge defines the chirality of the spiral corresponding to the sense of the circumrotation of the spiral. The spiral will circumrotate counterclockwise if σ has a positive value, while it will circumrotate clockwise if the σ has a negative value. The absolute value $|\sigma|$ is equal to the number of the arms of the spiral.

In our experiments, it is found that the topological charge of the spiral pattern can be changed when the spiral interacts with dislocations.

1. Dislocation in spiral pattern

In general, spiral patterns are not perfect, due to the presence of defects such as grain boundaries (line defects) and topological point defects (dislocations) [21]. The nucleation, motion, and annihilation of dislocations are essential for many pattern-selection processes, which are initiated by modulation instabilities [4]. Dislocations govern the ordering kinetics of initially disordered patterns [22] and sustain in defect turbulent systems the perpetual reordering of the plan forms [23]. Dislocation presents a simple realization of topological singularities in a field description of continuous extended systems [24].

In our experiment, the stripe and the spiral have a characteristic to keep wave-vector q_c invariable. As shown in Fig. 7, the stripe tends to be perpendicular to the sidewall when the applied voltage is high enough. It makes the wave vector of the fringe region smaller than the certain value q_c. A dislocation is created at the fringe region to retain the certain wave vector. It can modulate the local wave vector of the patterns when moving to the region where the local wave vector is smaller than some certain value.

By using the generalized Swift-Hohenberg equations [25], it is well known that dislocations are driven by a superposition of two independent forces. One is the Peach-Koehler (PK) force, which describes the tendency of the system to develop towards a striped pattern with an optimal average wave number [26,27]. Roughly speaking, it corresponds to an energy minimization principle. The other is the advection force. It is due to a long-range pressure field, caused by strong roll curvature gradients in the vicinity of a dislocation, which excites a flow field with a finite vertical average (mean flow) [28]. For a certain wave number q_c the two forces balance and a single dislocation is stationary. In most cases, the two forces do not balance, and the dislocation will move.

In the free boundary condition, the dislocation frequently comes from the exterior of the spiral. It creates an additional roll at the periphery of the spiral when it meets the spiral. The interaction of this additional roll with the spiral can change the topological charge of the spiral pattern. In the confined boundary condition, the dislocations are created at the periphery of the spiral pattern.

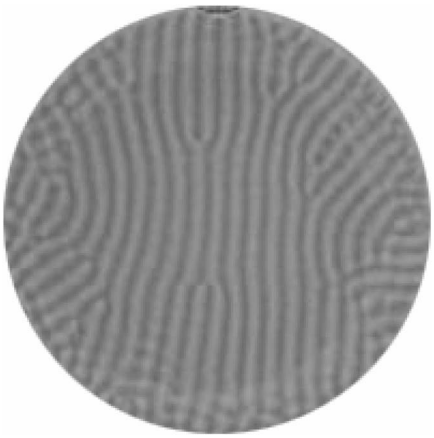

FIG. 7. The dislocations in stripe pattern. The discharge parameters: $p=760$ Torr, $d=1.4$ mm, $f=60$ kHz, $t_{\mathrm{exp}}=40$ ms, $U=3100$ V, $\chi=1.03\%$, and free boundary condition. The diameter of discharge area is 65 mm.

Sometimes, a dislocation pair can be created in the interior of the spiral pattern where the local wave vector is smaller than a certain value. Figure 2(a) shows a type of dislocation pair, also referred to as a bound state [29]. Another type of dislocation pair observed frequently is given in Fig. 8. As can be seen, due to meandering, the spiral moves toward the left, compressing the roll on one side while dilating it on the other side [Fig. 8(a)]. When the wave number of the compressed region increases beyond the skewed-varicose (SV) instability [30], a dislocation pair nucleates to decrease the wave number. One of the dislocation pairs moves to the center of the spiral to change the topological charge of the spiral while the other glides outward. Then the single-armed spiral finally becomes a double-armed spiral [Fig. 8(c)].

2. Transitions between the n-armed spirals

The number of the spiral arms can be changed as a result of the dislocation interacting with the spiral through gliding into the center of the spiral pattern.

Figure 9 shows how the dislocation makes a single-armed spiral become a double-armed spiral. The dislocation makes

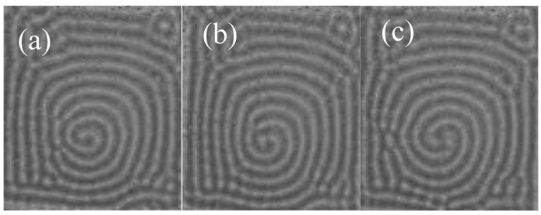

FIG. 8. The dislocation pair in the spiral. The discharge parameters: $p=760$ Torr, $d=1.4$ mm, $f=60$ kHz, $t_{\mathrm{exp}}=40$ ms, $U=3100$ V, $\chi=1.03\%$, and confined boundary condition. In this case, the boundary is rectangular with 40×45 mm.

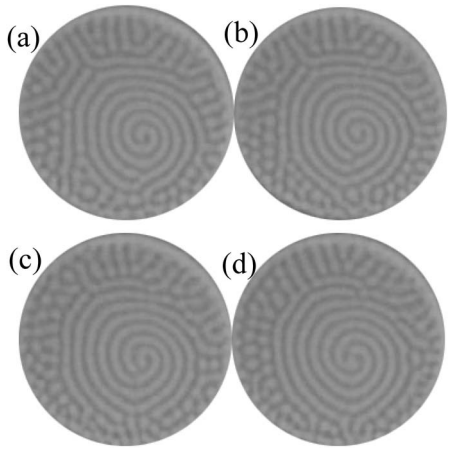

FIG. 9. Transition from a single-armed spiral to a double-armed spiral. The discharge parameters: $U=3100$ V, $\chi=1.16\%$, $p=760$ Torr, $d=1.4$ mm, $f=60$ kHz, $t_{exp}=40$ ms, and free boundary condition. Pictures are separated by 1/15 s. The diameter of discharge area is 65 mm.

the outset roll break down into two parts. One that connects with the dislocation becomes a new roll of the spiral, while the other part moves towards the center and becomes a new dislocation [Fig. 9(a)]. The new dislocation makes the nearby roll break down [Fig. 9(b)]. This process will continue until the dislocation moves into the core of the spiral. Then a double-armed spiral forms [Fig. 9(d)].

As shown in Fig. 10(a), a double-armed spiral transits into a single-armed spiral through a dislocation perturbing the spiral. The dislocation moves into the center [Figs. 10(a) and 10(b)]. The roll connecting with the dislocation loses its tip [Fig. 10(c)]. The isolated tip connects with the other tip and becomes the core of the newly-formed spiral, and then a single-armed spiral forms [Fig. 10(d)].

3. Transitions between the spiral and the target

In the transition spiral–target–spiral, the rotation direction of the spiral may change, which has also been found in dc driven planar semiconductor-gas discharge [17,18]. Whether

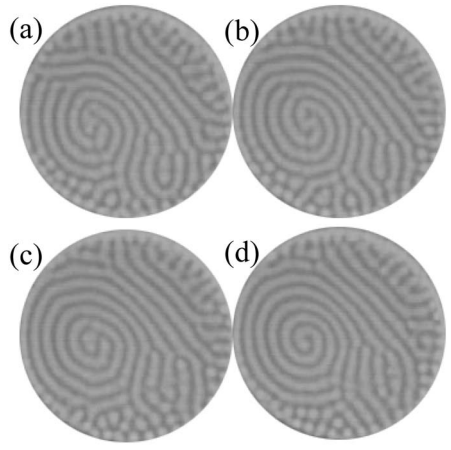

FIG. 10. Transition from a double-armed spiral to a single-armed spiral. The parameters are the same as that in Fig. 9.

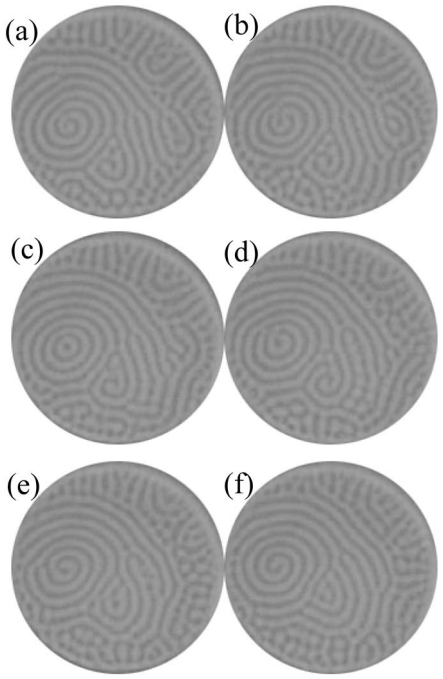

FIG. 11. Transition spiral → target → spiral. The rotation direction of final spiral (f) is the same as that of initial spiral (a). Pictures are separated by 1/15 s. The discharge parameters: $U=3300$ V, $\chi=1.16\%$, $p=760$ Torr, $d=1.4$ mm, $f=60$ kHz, $t_{exp}=40$ ms, and free boundary condition. The diameter of discharge area is 65 mm.

the rotation direction is changed or not depends on the feature of the middle state (target). The rotation direction does not change if the target does not create a new core as shown in Fig. 11. Otherwise, the rotation direction of the spiral will change. Such a process can be seen in Fig. 12. The new core propagates outward and becomes an additional circular roll [Figs. 12(c) and 12(d)]. Then the roll breaks down. One tip connects with the nearby roll while the other becomes the core of the spiral and the dislocation is the tail of the spiral [Fig. 12(f)]. In this case, the rotation direction of the spiral changes from counterclockwise to clockwise.

D. Spiral wavelength variation

In our experiments, it is found that the spiral wavelength in the confined boundary condition is related to gas composition but not dependent upon applied voltage.

As shown in Fig. 6, patterns undergo concentric rings–spiral pattern–stripe pattern as the applied voltage increases, but the average distance between consecutive rolls of these patterns is kept at 2.40 mm. Thus the wavelength of rolls (spiral, target, and stripe) observed in our experiment is independent of the applied voltage.

It is found that the wavelength of the rolls is related to gas composition. Figure 13 gives the wavelength λ as a function of air concentration χ in a mixture of argon and air. It shows that the wavelength decreases with the increases of air concentration. The value of the spiral wavelength in Fig. 13 is the average result of repetitious measurements. The biggest deviation has been taken as the error bar in Fig. 13.

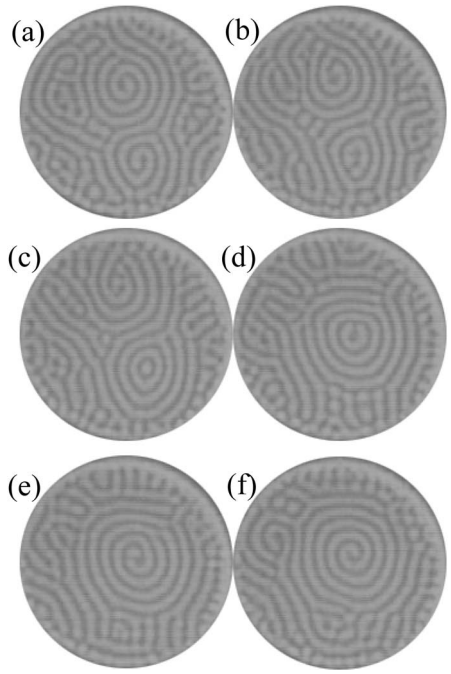

FIG. 12. Transition spiral → target → spiral. The rotation direction of final spiral (f) is opposite to that of initial spiral (a). Sequence of images: (a) $t=0$ s; (b) $t=1/15$ s; (c) $t=2/15$ s; (d) $t=4/15$ s; (e) $t=6/15$ s; (f) $t=8/15$ s. The discharge parameters: $U=3100$ V, $\chi=1.16\%$, $p=760$ Torr, $d=1.4$ mm, $f=60$ kHz, $t_{\mathrm{exp}}=40$ ms, and free boundary condition. The diameter of discharge area is 65 mm.

E. Spiral defect chaos

No matter what boundary condition is used in our experiments, a spiral defect chaos state has been observed. It is a spatially disorganized time-dependent state consisting of many localized rotating spirals and many defects as shown in Fig. 2(h). Usually the spirals are created and destroyed in the interior of the cell well away from boundary. Individual spirals typically rotate several times while translating a distance comparable to their diameter before being destroyed.

IV. CONCLUSIONS

In conclusion, a variety of spiral patterns such as single-armed spiral, dipole spirals, target pattern, multiarmed spiral, and spiral defect chaos state have been observed in ac-driven gas discharge. In the free boundary condition, the spiral pattern arises from a stripe pattern by increasing the applied voltage. Two types of instability, core instability and notching instability, have been observed. In the confined boundary condition, the spiral pattern is formed by sidewall forcing. Concentric rings occur from the periphery of the cell to the interior through increasing the applied voltage. Then the dislocations interact with the target background, resulting in the formation of the spiral pattern.

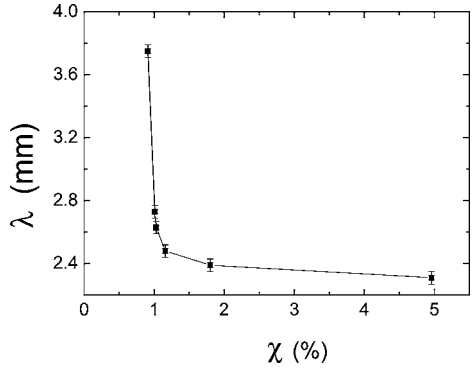

FIG. 13. The variation of the spiral wavelength as the function of air concentration. The discharge parameters: $p=760$ Torr, $d=1.4$ mm, $f=60$ kHz, and confined boundary condition.

Spiral motion depends on the boundary condition. In the free boundary condition, the spiral drifts upward. In the confined boundary condition, the spiral is a meandering spiral.

Dislocations and dislocation pairs are created to keep spiral wave-vector q_c invariable. The topological charge of the spiral pattern can be changed when the spiral interacts with the dislocations.

The spiral wavelength depends on the gas composition. It decreases rapidly with increase of air concentration in discharge gas for the fixed gap width d and the frequency of the applied voltage f.

The various spiral patterns, rich behavior, luminous feature, and convenient experimental time scale of the discharge make the ac-driven atmospheric pressure dielectric barrier discharge an excellent system for further studies of the spiral pattern. Further research is going on.

ACKNOWLEDGMENTS

This work is supported by the National Natural Science Foundation of China under Grant No. 10375015, the Key Project of Chinese Ministry of Education (No. 02020), Committee of Science and Technology, Hebei Province, China under Grant No. 01212180, Bureau of Education, Hebei Province, China under Grant No. B2001112, and the Natural Science Foundation of Hebei Province, China under Grant No. A2004000086. We thank Professor Wei Yu for his help.

[1] A. N. Zaikin and A. M. Zhabotinsky, Nature (London) **225**, 535 (1970).
[2] J. D. Murray, *Mathematical Biology* (Springer, Berlin, 1993).
[3] M. Assenheimer and V. Steinberg, Phys. Rev. Lett. **70**, 3888 (1993); Nature (London) **367**, 345 (1994).
[4] M. C. Cross and P. Hohenberg, Rev. Mod. Phys. **65**, 851 (1993).
[5] S. V. Kiyashko, L. N. Korzinov, M. I. Rabinovich, and L. S. Tsimring, Phys. Rev. E **54**, 5037 (1996).
[6] John R. de Bruyn, B. C. Lewis, M. D. Shattuck, and Harry L.

Swinney, Phys. Rev. E **63**, 041305 (2001).
[7] M. Bestehorn, M. Frantz, R. Friedrich, and H. Haken, Phys. Lett. A **174**, 48 (1993).
[8] A. C. Newell and T. Passot, Phys. Rev. Lett. **68**, 1846 (1992).
[9] M. C. Cross, Physica D **97**, 65 (1996).
[10] W. Breazeal, K. M. Flynn, and E. G. Gwinn, Phys. Rev. E **52**, 1503 (1995).
[11] I. Muller, C. Punset, E. Ammelt, H.-G. Purwins, and J. P. Boeuf, IEEE Trans. Plasma Sci. **27**, 20 (1999).
[12] E. L. Gurevich, A. L. Zanin, A. S. Moskalenko, and H.-G. Purwins, Phys. Rev. Lett. **91**, 154501 (2003).
[13] L. F. Dong, Z. Q. Yin, L. Wang, G. S. Fu, Y. F. He, Z. F. Chai, and X. C. Li, Thin Solid Films **435**, 120 (2003).
[14] L. F. Dong, Z. G. Mao, Z. Q. Yin, and J. X. Ran, Appl. Phys. Lett. **84**, 5142 (2004).
[15] L. F. Dong, Y. F. He, Z. Q. Yin, and Z. F. Chai, Chin. Phys. Lett. **20**,1524 (2003).
[16] U. Kogelschatz, IEEE Trans. Plasma Sci. **30**, 1400 (2002).
[17] Yu. A. Astrov, I. Muller, E. Ammelt, and H.-G. Purwins, Phys. Rev. Lett. **80**,5341 (1998).
[18] E. L. Gurevich, Yu. A. Astrov, and H.-G. Purwins, J. Phys. D **38**, 468 (2005).
[19] M. C. Cross and Y. Tu, Phys. Rev. Lett. **75**, 834 (1995).
[20] E. Bodenschatz, J. R. de Bruyn, G. Ahlers, and D. S. Cannell, Phys. Rev. Lett. **67**, 3078 (1991).
[21] A. C. Newell, T. Passot, and J. Lega, Annu. Rev. Fluid Mech. **25**, 399 (1993).
[22] C. Harrison, D. H. Adamson, Z. Cheng, J. M. Sebastian, S. Sethuraman, D. A. Huse, R. A. Register, and P. M. Chaikin, Science **290**, 1558 (2000).
[23] K. E. Daniels and E. Bodenschatz, Phys. Rev. Lett. **88**, 034501 (2002).
[24] L. M. Pismen, *Vortices in Nonlinear Fields* (Clarendon Press, Oxford, 1999).
[25] J. B. Swift and P. C. Hohenberg, Phys. Rev. A **15**, 319 (1977).
[26] E. D. Siggia and A. Zippelius, Phys. Rev. A **24**, 1036 (1981).
[27] G. Tesauro and M. C. Cross, Phys. Rev. A **34**, 1363 (1986).
[28] K. H. Chiam, M. R. Paul, M. C. Cross, and H. S. Greenside, Phys. Rev. E **67**, 056206 (2003).
[29] E. Bodenschatz, D. S. Cannell, J R de Bruyn, Y. Hu, K. Lerman, and G. Ahlers, Physica D **61**, 77 (1992).
[30] F. H. Busse and R. M. Clever, J. Fluid Mech. **91**, 319 (1979).